

Consecutive and Extensive Transition of Luminescent Color of an Organic Solid Material by Applying High Pressure

Junjie Guan, Xingyu Tang, Chunfang Zhang, Kuo Li, Xiaohuan Lin, Lin Wang, Hyun Hwi Lee, Jiali Xu,* Haiyan Zheng,* and Ho-kwang Mao

Cite This: *J. Phys. Chem. C* 2020, 124, 14911–14917

Read Online

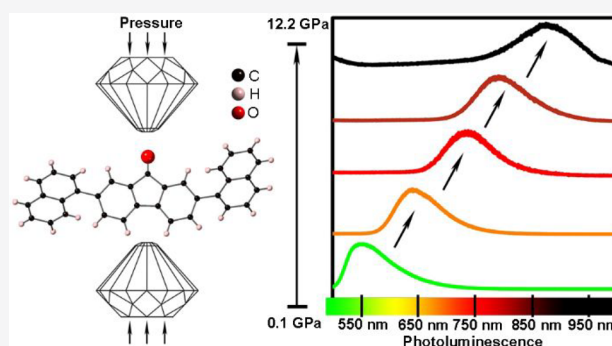
ACCESS |

Metrics & More

Article Recommendations

Supporting Information

ABSTRACT: By compressing the organic solid luminescent material 2,7-di(naphthalen-1-yl)fluorenone (1-DNFO), a consecutive and massive modulation of its UV–vis absorption and photoluminescence spectra has been achieved. In particular, the photoluminescence peak shifts from the visible (548 nm) to the near-IR region (879 nm). In situ high-pressure synchrotron X-ray diffraction studies indicate that the tremendous photoluminescence redshift of 1-DNFO with a parallel packing mode results from the enhancement of intermolecular interaction, which is caused by the decrease of unit cell volume and intramolecular dihedral angle. Additionally, a time-dependent density functional theory study shows that the enhancement of intermolecular interaction under high pressure should be responsible for the dramatic redshift of the absorption and emission spectra. For comparison, the analogue 2,7-di(naphthalen-2-yl)fluorenone (2-DNFO) with an interlaced packing mode shows the relatively small-scale photoluminescence redshift under compression, due to the difference of molecular arrangements. Our research manifests that the optical properties of organic optical crystals with effective $\pi\cdots\pi$ interaction are more sensitive to external pressure, which may have the potential application for multicolor luminescent materials and devices.



INTRODUCTION

In recent years, organic solid luminescent materials have drawn broad attention on account of their wide applications in optoelectronic devices, data recording, biological sensing and imaging.^{1–5} Based on the practical and urgent demands of multicolor displays,^{6,7} it is of significant importance to efficiently acquire the tunable luminescent color from the organic-based light emission. The diverse luminescent properties of organic optical materials depend highly on the molecular conformations, arrangements and interactions.^{8–11} For example, the self-assembled structures of organic dyes can limit their intramolecular movements of groups, and they can thus enhance the fluorescence intensity.¹² The restriction of molecular vibrations in organic chromophores might result in the drastic increase of emission intensity too.¹³ The lattice deformation of perovskite-structure can also spatially limit excitons and observably improve fluorescence quantum yield.¹⁴ The enhancement of the intermolecular $\pi\cdots\pi$ stacking interaction in crystal structures of organic dyes have been reported to shift the luminescence to longer wavelength and decrease the luminescence intensity.¹⁵ However, it is still hard to achieve large-scale multicolor modulation of luminescence by conventional stimuli such as solution processes, cocrystal strategies or grinding methods.^{16–19} Recently, the burgeoning high-pressure techniques have been recognized as a direct and

efficient tool to alter the crystal structures and molecular interaction, and can thus tune the optoelectronic properties of the materials.^{20–28} Along with this strategy, applying pressure to organic luminescent materials is expected to be an effective new method to obtain the particular luminescent properties. Meanwhile, a deep understanding of the structure–property relationship under high pressure is very important for designing and regulating the functional optical materials.

Fluorenone derivatives with strong light-emission in the solid state have been explored in the tunable luminescent fields.^{29–33} By controlling the processing conditions such as the drop-casting parameters of solution,²⁹ or the contents of good and poor solvents during recrystallization,^{31,34} regulable light-emitting performance of fluorenone derivatives with different molecular packing modes can be obtained. Here, the fluorenone derivatives substituted by naphthyl group were chosen to explore the photobehaviors under high pressure due to their advantages of long organic π -conjugated structures,

Received: April 16, 2020

Revised: June 5, 2020

Published: June 8, 2020



flexible naphthyl groups and enough space for compression. The crystals of 2,7-di(naphthalen-1-yl)fluorenone (1-DNFO) and 2,7-di(naphthalen-2-yl)fluorenone (2-DNFO) were obtained via the same recrystallization method. By applying pressure to 1-DNFO, the in situ UV–vis absorption and photoluminescence spectra exhibited a tremendous and continuous redshift from visible light to the near-infrared region. The enhancement of intermolecular interaction caused by the decrease of cell volume and dihedral angle between fluorenone group and naphthyl group was found to be responsible for such a dramatic redshift in both the absorption and emission spectra. As a contrast, the 2-DNFO with the fluorenone group connected with the position 2 of naphthyl moiety shows an interlaced packing mode and an inconspicuous redshift was observed under compression compared to that of the 1-DNFO with the parallel arrangement. Time-dependent density functional theory (TD-DFT) studies suggest that the enhanced intermolecular interaction upon compression is the essential reason for the decrease of excited energy. The organic optical molecules with more effective $\pi\cdots\pi$ interaction were proved to be an efficient pressure-responsive molecular switch for tuning the absorption and emission properties.

EXPERIMENTAL SECTION

Sample Preparation and High-Pressure Generation.

The synthesis of the model compounds and the fabrication of the crystals were described in our earlier publications.^{30,32} 1-DNFO and 2-DNFO were synthesized through the Suzuki coupling reaction. The samples were purified by chromatography method and recrystallization and then ground into powder samples for high pressure experiments. The purity was confirmed by powder X-ray diffraction (XRD) at ambient pressure. 1-DNFO shows the β -phase with the Pc group, and 2-DNFO shows the α -phase with the $P2_1/n$ group.³² The symmetric diamond anvil cell (DAC) (diameter of anvil culet: 300 μm) was used to generate high pressure. T301 stainless steel gaskets were preindented to a thickness of 60 μm and holes with a diameter of 120 μm were drilled at the center of the indentations to act as the sample chamber. The ruby fluorescence method was used to measure the pressure.³⁵ All in situ high-pressure experiments were performed under room temperature.

In Situ Optical Spectra and XRD Measurements under High Pressure. In situ UV–vis absorption experiments were conducted by using a deuterium-halogen light source (78 VA). Silicone oil was loaded to act as the pressure transmitting medium and its absorption was used for background calibration. In situ photoluminescence spectra were collected under the excitation of 488 nm laser with a Renishaw Raman microscope (RM1000). In situ synchrotron XRD experiments were performed by using a focused monochromatic X-ray beam (0.69265 \AA) of 5A-MS-XRS beamline facility at Pohang Accelerator Laboratory. The data were collected by a Mar345 detector under the calibration of CeO_2 standard sample. The preliminary data reduction of XRD patterns was conducted with the Dioptas program,³⁶ and the Rietveld refinement of XRD data was performed by using the Jana 2006 program.³⁷ The 1-DNFO molecule was set as a rigid body except for the dihedral angle between the naphthyl ring and the fluorenone group. The thermal factors were fixed during the refinement.

Theoretical Calculation Details. The TD-DFT calculations were performed by using Gaussian 09 D01³⁸ with the B3LYP functional^{39,40} and the 6-311G* basis set.⁴¹ The first five excited states were selected for the simulated absorption spectra. The representative aggregates of 1-DNFO including four adjacent molecules were chosen from the crystal structures under 0.2 and 8.3 GPa for conducting the TD-DFT calculations. The high-pressure crystal structures of 1-DNFO at 0.2 and 8.3 GPa were obtained through the Rietveld refinement of XRD data. No further optimizations were carried out.

RESULTS AND DISCUSSION

Switching Optical Behaviors under High Pressure.

The in situ high-pressure UV–vis absorption and photoluminescence spectra were collected to investigate the pressure-responsive optical properties of the 1-DNFO. As shown in Figure 1a, the longest-wavelength absorption peak of 1-DNFO is in the visible light region at around 497 nm under

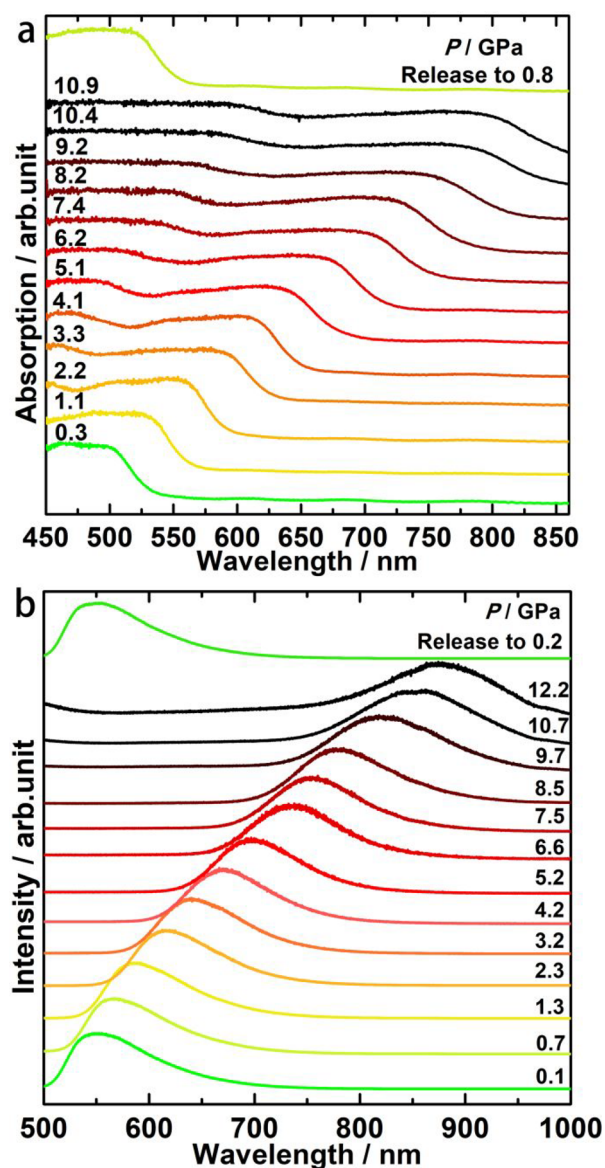


Figure 1. In situ high-pressure (a) absorption and (b) photoluminescence spectra of 1-DNFO.

0.3 GPa. With further compression, the absorption spectra show distinct and continuous redshift to longer wavelengths. At 10.9 GPa, the corresponding absorption band crosses the visible light region and finally reaches 800 nm. Meanwhile, the photoluminescence spectra exhibit an emission peak centered at 548 nm under 0.1 GPa (Figure 1b). Through the application of pressure, the emission peak red-shifts continuously and finally moves to 879 nm at 12.2 GPa. In particular, the emission peak crosses over 300 nm in wavelength and finally moves from the visible light to the near-infrared region. Upon releasing the pressure, both the absorption and emission spectra turned back to their original states (Figure 1, parts a and b), which indicated the optical variation was reversible under high pressure. Figure 2 shows the variations of

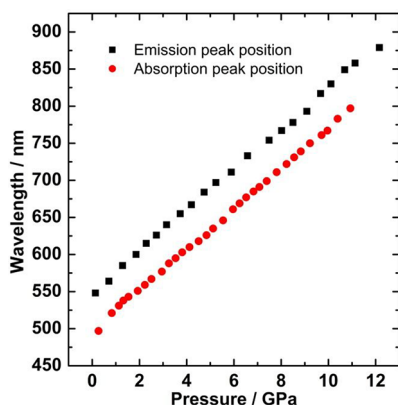


Figure 2. Evolution of longest-wavelength absorption and emission peak positions of 1-DNFO with increasing pressure.

absorption and emission peak positions with increasing pressure, which undergo a nice consecutive process under compression and reveal a good linear relation with pressure. This indicates that no phase transition happened during the compression. Such a sustaining and large-scale transformation of emission and absorption from visible to the near-infrared region is hardly accomplished by conventional methods including solution process or mechanical grinding. The details of structural evolution for 1-DNFO need to be investigated under high pressure for analyzing this special optical phenomenon, and the structure–property relationship under high pressure will provide deep insight into potential optical applications.

Structural Evolution under High Pressure. Synchrotron XRD experiments were used to analyze the relationship between the crystal structures and optical properties under high pressure (Figure 3a). The XRD pattern of 1-DNFO at 0.2 GPa was well fitted by the β -phase structure of 1-DNFO³² through Rietveld refinement, with a Pc space group (Figure 3b) and the corresponding unit cell parameters ($a = 19.268(10)$ Å, $b = 3.9318(6)$ Å, $c = 14.912(6)$ Å, $\alpha = 90^\circ$, $\beta = 112.80(3)^\circ$, and $\gamma = 90^\circ$). The XRD peaks at 0.2 GPa were marked using Miller indices, as shown in the Figure 3a. With increasing pressure, all the XRD peaks of 1-DNFO moved to higher 2θ without generating new XRD peaks. By conducting the Rietveld refinement of 1-DNFO under high pressures, the cell volume continuously decreases with increasing pressure (Figure 4a). The inset in Figure 4a gives the dependence of lattice constants with pressure. The continuity in variations of the XRD patterns, unit cell volume and lattice constants

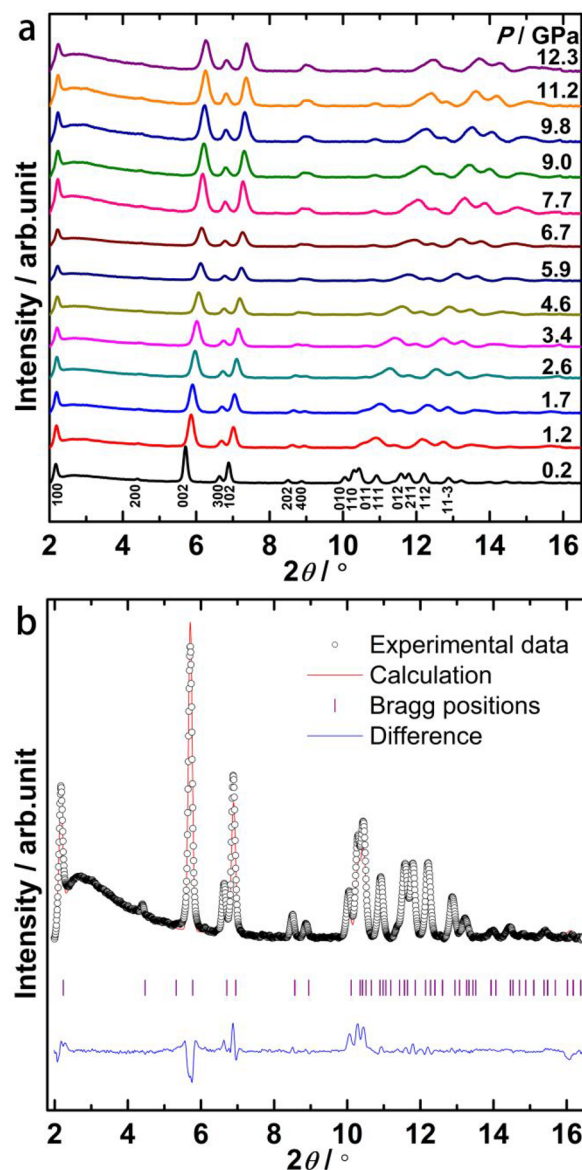


Figure 3. (a) Selected synchrotron XRD patterns of 1-DNFO under compression. (b) Rietveld refinement of 1-DNFO at 0.2 GPa.

affirmed that there was no phase transition of 1-DNFO during compression. This is consistent with the results of absorption and emission measurements. Meanwhile, the dihedral angle between the fluorenone and naphthyl groups also decreased under compression (Figure 4b). The decrease of unit cell volume and dihedral angle results in the obvious decrease of $\pi\cdots\pi$ stacking distance between aromatic rings (Figure S1), which indicates the enhancement of the intermolecular $\pi\cdots\pi$ interaction and thus lead to the obvious redshift of absorption and emission.^{13,15}

For comparison, the in situ photoluminescence spectra of 2-DNFO were also measured under high pressure (orange solid line in Figure 5a). At 0.1 GPa, the corresponding emission peak of 2-DNFO was at around 600 nm, which shows a longer emission wavelength at the similar pressure compared to 1-DNFO due to the better coplanarity of molecular conformation (Figure 5b). However, 2-DNFO displayed a relatively small-scale redshift of emission (from 602 to 703 nm, about 100 nm), in contrast to the large-scale redshift of 1-

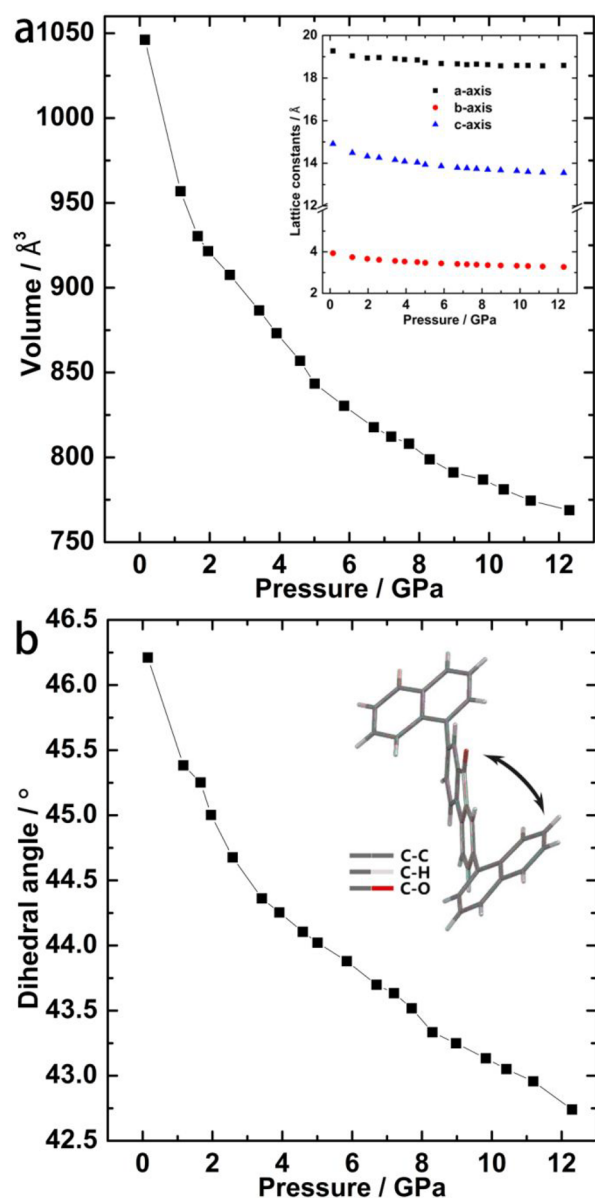


Figure 4. (a) Decrease of unit cell volume of 1-DNFO with increasing pressure (inset: variations of lattice parameters). (b) Evolution of dihedral angle between fluorenone and naphthyl groups under different pressures.

DNFO as indicated by the black dot lines in Figure 5a. The in situ UV–vis absorption spectra also show the localized modulation of absorption under compression (Figure S2). The synchrotron XRD patterns indicated no phase transition occurred in 2-DNFO under high pressure (Figure S3). Therefore, the differences in molecular conformation and arrangement of adjacent molecules between 1-DNFO and 2-DNFO are the major reasons for the distinguished optical properties upon increasing pressure. In 1-DNFO, the same aromatic rings (naphthyl or fluorenone moieties) are stacked in a parallel packing mode in the molecular aggregate (Figure 5b). Along the crystallographic *b*-axis of the unit cell, 1-DNFO shows molecular chains built by intermolecular $\pi\cdots\pi$ stacking interaction (see details in Figure S4). The molecular chains are mainly connected by the C–H \cdots O hydrogen bonds. Under compression, 1-DNFO can modulate the optical spectra to longer wavelengths through decreasing the unit cell volume,

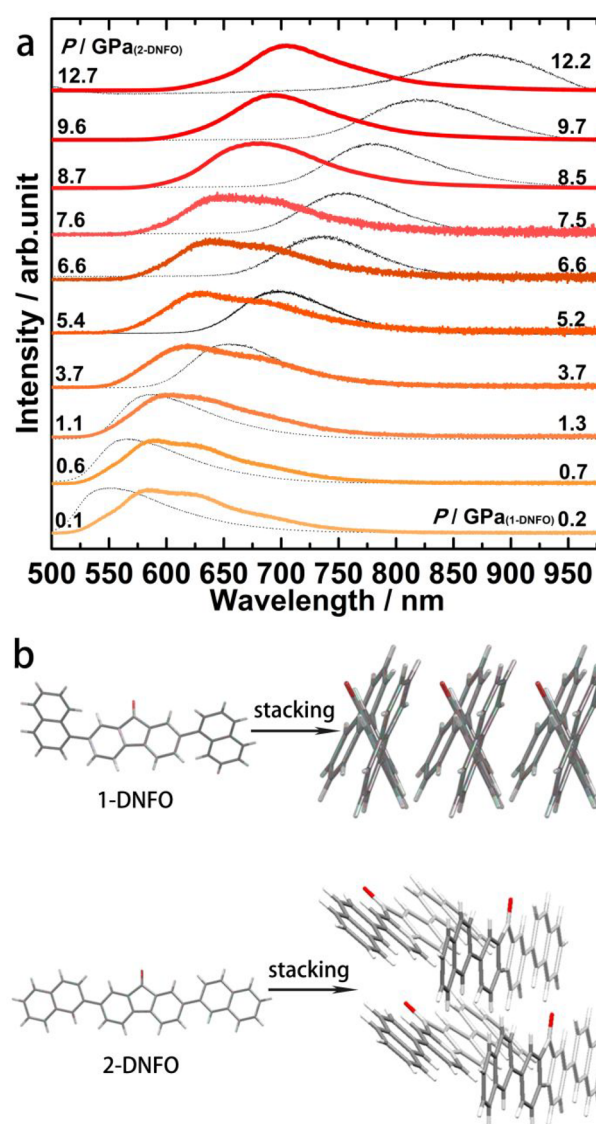


Figure 5. (a) Selected in situ high-pressure photoluminescence spectra of 2-DNFO (orange solid lines), in comparison with the photoluminescence spectra of 1-DNFO under the same pressure (the black dotted lines). (b) Molecular arrangement and conformation of 1-DNFO and 2-DNFO under ambient conditions.

dihedral angle and intermolecular distance and thus enhance the intermolecular $\pi\cdots\pi$ interaction (see details in Figure S5). Nevertheless, the analogue, 2-DNFO molecules are arranged in an interlaced packing mode (Figure 5b). In the molecular aggregate of 2-DNFO, the molecular chains with interlaced packing mode are mainly built by the intermolecular C–H \cdots π repulsion interaction (see details in Figure S4). The molecular chains are connected by C–H \cdots O hydrogen bond. No obvious intermolecular $\pi\cdots\pi$ stacking interaction was observed in 2-DNFO. Hence, the application of pressure can not efficiently enhance the intermolecular interaction of 2-DNFO or massively modulate the photoluminescence. The comparison between the 1-DNFO and 2-DNFO shows the crystal structure with more effective $\pi\cdots\pi$ interaction is more sensitive to pressure in modulating optical properties.

Theoretical Studies. TD-DFT calculations have been conducted to provide further comprehending of the massive redshift of the optical spectra for 1-DNFO. The absorption

spectra were simulated by the TD-DFT method and aggregates containing four adjacent 1-DNFO molecules were chosen based on the Rietveld refinement results at 0.2 and 8.3 GPa, respectively (Figure 3b, Figure S6 and Figure S7). As shown in Figure 6a, the longest-wavelength absorption peaks under 0.2

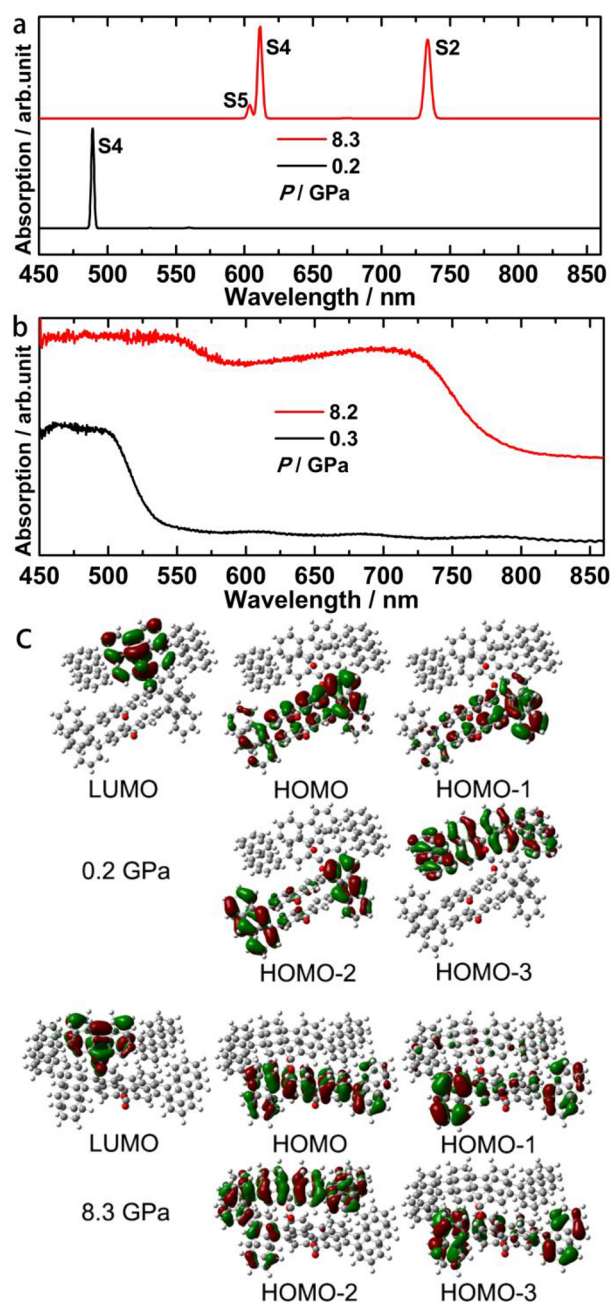


Figure 6. (a) TDDFT-calculated absorption spectra of 1-DNFO with the aggregates of four chosen molecules at selected pressures. (b) Corresponding in situ experimental values of absorption spectra at the corresponding pressures. (c) Simulated molecular orbitals of 1-DNFO under 0.2 and 8.3 GPa, respectively.

and 8.3 GPa were simulated to be at 489 and 733 nm, respectively. The simulated results are in good agreement with the results observed in experiment (at around 497 and 722 nm under 0.3 and 8.2 GPa, respectively, as shown in Figure 6b). The small difference between the simulated and experimental results might come from the limitation of the computational

method and the simulated models.^{42,43} In addition, the strong peak at 489 nm under 0.2 GPa, mainly derive from the S4 excited state of 1-DNFO, corresponding to the transition from the third molecular orbital below the highest occupied molecular orbital (HOMO-3) to the lowest unoccupied molecular orbital (LUMO). On the other hand, the strong peak centered at 733 nm at 8.3 GPa is from the S2 state, which corresponds a majority transition (79.8%) from HOMO-2 to LUMO and a minority transition (16.8%) from HOMO-1 to LUMO. The additional simulated absorption bands at about 611 and 603 nm under 8.3 GPa correspond to the S4 and S5 states, respectively (see Table 1 for the details of the excited states).

Table 1. Time-Dependent Density Functional Theory calculated values for the five lowest-lying excited singlet states of 1-DNFO at 0.2 and 8.3 GPa, respectively

state	excitation energy (EE) (eV)	oscillator strengths (OS)	dominant orbital transitions contributions (DOTC)
0.2 GPa			
S1	2.2159	0.0002	H→L (96.7%) ^a
S2	2.3342	0.0000	H-1→L (92.7%)
S3	2.4236	0.0000	H→L+1 (94.1%)
S4	2.5346	0.0434	H-3→L (94.8%)
S5	2.5480	0.0000	H-1→L+1 (93.5%)
8.3 GPa			
S1	1.4041	0.0007	H→L (98.4%)
S2	1.6899	0.0345	H-2→L (79.8%), H-1→L (16.8%)
S3	1.8385	0.0001	H-2→L (17.4%), H-1→L (76.7%)
S4	2.0280	0.0404	H→L+1 (21.7%), H→L+2 (68.0%)
S5	2.0535	0.0059	H-3→L (83.9%)

^aH and L represent the highest occupied molecular orbital (HOMO) and lowest unoccupied molecular orbital (LUMO), respectively.

As shown in Figure 6c, at 0.2 and 8.3 GPa, the LUMO is mainly distributed on the fluorenone group, and HOMO, HOMO-1, HOMO-2 and HOMO-3 are distributed over the whole 1-DNFO molecule. However, compared to the orbitals at 0.2 GPa, more significant overlap of the wave function between the neighbor molecules can be observed in HOMO-1 and HOMO-2 when compressing to 8.3 GPa. This signifies the enhancement of the intermolecular interaction between neighboring molecules upon compression, which results in the decrease of energy gap between the LUMO and HOMO-1 and HOMO-2 of 1-DNFO (Table S1) and thus contributes to the long-wavelength absorption and emission observed in 1-DNFO.

CONCLUSION

Our studies demonstrate high pressure is a powerful tool to drastically modulate the optical properties of organic molecular crystals. Under the limitation effect of high pressure, the 1-DNFO exhibits prominent and continuous redshift of absorption and emission spectra. High pressure leads to the decrements of cell volume and dihedral angle between groups and the enhancement of intermolecular interaction. By analyzing the TD-DFT calculated results under different pressures, we find strong evidence that the compression makes the enhancement of the intermolecular $\pi\cdots\pi$ interactions which causes the decrease of energy gap between the

LUMO and HOMO–1 and HOMO–2 and results in longer absorption and luminescence spectra. As a comparison, the 2-DNFO with interlaced packing mode shows small-scale redshift. Our work highlights the high pressure is an effective method to tune the optical properties by modification of the intermolecular interaction and the one with more effective $\pi\cdots\pi$ interaction will be more sensitive to the pressure. This study provides significant and valuable insight into the development of new high efficiency multicolor display materials and devices.

■ ASSOCIATED CONTENT

SI Supporting Information

(PDF). The Supporting Information is available free of charge at <https://pubs.acs.org/doi/10.1021/acs.jpcc.0c03400>.

Figure S1, $\pi\cdots\pi$ distance between aromatic rings of 1-DNFO under different pressures; Figure S2, selected in situ UV–vis absorption spectra of 2-DNFO under different pressures; Figure S3, synchrotron XRD patterns of 2-DNFO with increasing pressure; Figure S4, selected molecular aggregates of 1-DNFO and 2-DNFO in the unit cell; Figure S5, $\pi\cdots\pi$ distance and dihedral angle of selected molecular aggregates of 1-DNFO under 0.2 and 8.3 GPa, respectively; Figure S6, Rietveld refinement result of 1-DNFO at 8.3 GPa; Figure S7, selected models of molecular aggregates of 1-DNFO under 0.2 and 8.3 GPa, respectively; and Table S1, selected molecular orbital energy values of 1-DNFO at 0.2 and 8.3 GPa, respectively, obtained from Time-Dependent Density Functional Theory calculation (PDF)

■ AUTHOR INFORMATION

Corresponding Authors

Jialiang Xu – School of Chemical Engineering and Technology, Tianjin University, Tianjin 300350, P. R. China; School of Materials Science and Engineering, Nankai University, Tianjin 300350, P. R. China; orcid.org/0000-0003-2441-4809; Email: jialiang.xu@nankai.edu.cn

Haiyan Zheng – Center for High Pressure Science and Technology Advanced Research (HPSTAR), Beijing 100094, P. R. China; orcid.org/0000-0002-4727-5912; Email: zhenghy@hpstar.ac.cn

Authors

Junjie Guan – Center for High Pressure Science and Technology Advanced Research (HPSTAR), Beijing 100094, P. R. China; School of Chemical Engineering and Technology, Tianjin University, Tianjin 300350, P. R. China

Xingyu Tang – Center for High Pressure Science and Technology Advanced Research (HPSTAR), Beijing 100094, P. R. China

Chunfang Zhang – College of Chemistry and Environmental Science, Hebei University, Baoding 071002, Hebei, P. R. China

Kuo Li – Center for High Pressure Science and Technology Advanced Research (HPSTAR), Beijing 100094, P. R. China; orcid.org/0000-0002-4859-6099

Xiaohuan Lin – Center for High Pressure Science and Technology Advanced Research (HPSTAR), Beijing 100094, P. R. China

Lin Wang – Center for High Pressure Science and Technology Advanced Research (HPSTAR), Beijing 100094, P. R. China; orcid.org/0000-0003-2931-7629

Hyun Hwi Lee – Pohang Accelerator Laboratory, POSTECH, Pohang 790-784, Republic of Korea

Ho-kwang Mao – Center for High Pressure Science and Technology Advanced Research (HPSTAR), Beijing 100094, P. R. China

Complete contact information is available at:

<https://pubs.acs.org/doi/10.1021/acs.jpcc.0c03400>

Author Contributions

The manuscript was written through contributions of all authors. All authors have given approval to the final version of the manuscript.

Notes

The authors declare no competing financial interest.

■ ACKNOWLEDGMENTS

This work was financially supported by the National Natural Science Foundation of China (21875006, 21771011, and 21773168), and “111 Project” of China (B18030). The authors also acknowledge the support from the Top 1000-Talents Award and the computational support from the High-Performance Computing Center of Hebei University.

■ REFERENCES

- (1) Yan, D.; Evans, D. G. Molecular Crystalline Materials with Tunable Luminescent Properties: from Polymorphs to Multi-component Solids. *Mater. Horiz.* **2014**, *1*, 46–57.
- (2) Grimsdale, A. C.; Leok Chan, K.; Martin, R. E.; Jokisz, P. G.; Holmes, A. B. Synthesis of Light-Emitting Conjugated Polymers for Applications in Electroluminescent Devices. *Chem. Rev.* **2009**, *109*, 897–1091.
- (3) Tessler, N.; Medvedev, V.; Kazes, M.; Kan, S.; Banin, U. Efficient Near-Infrared Polymer Nanocrystal Light-Emitting Diodes. *Science* **2002**, *295*, 1506–1508.
- (4) Boens, N.; Leen, V.; Dehaen, W. Fluorescent Indicators based on BODIPY. *Chem. Soc. Rev.* **2012**, *41*, 1130–1172.
- (5) Yan, Y.; Zhang, C.; Yao, J.; Zhao, Y. S. Recent Advances in Organic One-Dimensional Composite Materials: Design, Construction, and Photonic Elements for Information Processing. *Adv. Mater.* **2013**, *25*, 3627–3638.
- (6) Chiang, C.-L.; Tseng, S.-M.; Chen, C.-T.; Hsu, C.-P.; Shu, C.-F. Influence of Molecular Dipoles on the Photoluminescence and Electroluminescence of Dipolar Spirobifluorenes. *Adv. Funct. Mater.* **2008**, *18*, 248–257.
- (7) Friend, R. H.; Gymer, R. W.; Holmes, A. B.; Burroughes, J. H.; Marks, R. N.; Taliani, C.; Bradley, D. D. C.; Santos, D. A. D.; Bredas, J. L.; Logdlund, M.; et al. Electroluminescence in Conjugated Polymers. *Nature* **1999**, *397*, 121–128.
- (8) Mutai, T.; Satou, H.; Araki, K. Reproducible on-off Switching of Solid-state Luminescence by Controlling Molecular Packing through Heat-mode Interconversion. *Nat. Mater.* **2005**, *4*, 685–687.
- (9) Xu, J.; Semin, S.; Rasing, T.; Rowan, A. E. Organized Chromophoric Assemblies for Nonlinear Optical Materials: Towards (Sub)wavelength Scale Architectures. *Small* **2015**, *11*, 1113–1129.
- (10) Zhang, H.; Zheng, X.; Xie, N.; He, Z.; Liu, J.; Leung, N. L. C.; Niu, Y.; Huang, X.; Wong, K. S.; Kwok, R. T. K.; et al. Why Do Simple Molecules with “Isolated” Phenyl Rings Emit Visible Light? *J. Am. Chem. Soc.* **2017**, *139*, 16264–16272.
- (11) Zhang, H.; Zhang, Z.; Ye, K.; Zhang, J.; Wang, Y. Organic Crystals with Tunable Emission Colors Based on a Single Organic Molecule and Different Molecular Packing Structures. *Adv. Mater.* **2006**, *18*, 2369–2372.
- (12) Zhao, Z.; He, B.; Tang, B. Z. Aggregation-Induced Emission of Siloles. *Chem. Sci.* **2015**, *6*, 5347–5365.
- (13) Gu, Y.; Wang, K.; Dai, Y.; Xiao, G.; Ma, Y.; Qiao, Y.; Zou, B. Pressure-Induced Emission Enhancement of Carbazole: The Re-

striction of Intramolecular Vibration. *J. Phys. Chem. Lett.* **2017**, *8*, 4191–4196.

(14) Li, S.; Luo, J.; Liu, J.; Tang, J. Self-Trapped Excitons in All-Inorganic Halide Perovskites: Fundamentals, Status, and Potential Applications. *J. Phys. Chem. Lett.* **2019**, *10*, 1999–2007.

(15) Yao, Z.-Q.; Xu, J.; Zou, B.; Hu, Z.; Wang, K.; Yuan, Y.-J.; Chen, Y.-P.; Feng, R.; Xiong, J.-B.; Hao, J.; et al. A Dual-Stimuli-Responsive Coordination Network Featuring Reversible Wide-Range Luminescence-Tuning Behavior. *Angew. Chem., Int. Ed.* **2019**, *58*, 5614–5618.

(16) Dong, Y.; Xu, B.; Zhang, J.; Tan, X.; Wang, L.; Chen, J.; Lv, H.; Wen, S.; Li, B.; Ye, L.; et al. Piezochromic Luminescence Based on the Molecular Aggregation of 9,10-Bis((E)-2-(pyrid-2-yl)vinyl)-anthracene. *Angew. Chem., Int. Ed.* **2012**, *51*, 10782–10785.

(17) Lin, H.; Chang, X.; Yan, D.; Fang, W.-H.; Cui, G. Tuning Excited-State-Intramolecular-Proton-Transfer (ESIPT) Process and Emission by Cocrystal Formation: a Combined Experimental and Theoretical Study. *Chem. Sci.* **2017**, *8*, 2086–2090.

(18) Mei, J.; Leung, N. L. C.; Kwok, R. T. K.; Lam, J. W. Y.; Tang, B. Z. Aggregation-Induced Emission: Together We Shine, United We Soar! *Chem. Rev.* **2015**, *115*, 11718–11940.

(19) Yoon, S.-J.; Chung, J. W.; Gierschner, J.; Kim, K. S.; Choi, M.-G.; Kim, D.; Park, S. Y. Multistimuli Two-Color Luminescence Switching via Different Slip-Stacking of Highly Fluorescent Molecular Sheets. *J. Am. Chem. Soc.* **2010**, *132*, 13675–13683.

(20) Li, M.; Liu, T.; Wang, Y.; Yang, W.; Lü, X. Pressure Responses of Halide Perovskites with Various Compositions, Dimensionalities, and Morphologies. *Matter Radiat. Extremes* **2020**, *5*, 018201.

(21) Yoo, C.-S. Chemistry under Extreme Conditions: Pressure Evolution of Chemical Bonding and Structure in Dense Solids. *Matter Radiat. Extremes* **2020**, *5*, 018202.

(22) Li, N.; Gu, Y.; Chen, Y.; Zhang, L.; Zeng, Q.; Geng, T.; Wu, L.; Jiang, L.; Xiao, G.; Wang, K.; et al. Pressure-Induced Emission Enhancement and Piezochromism of Triphenylethylene. *J. Phys. Chem. C* **2019**, *123*, 6763–6767.

(23) Guan, J.; Zhang, C.; Gao, D.; Tang, X.; Dong, X.; Lin, X.; Wang, Y.; Wang, X.; Wang, L.; Lee, H. H.; et al. Drastic Photoluminescence Modulation of an Organic Molecular Crystal with High Pressure. *Mater. Chem. Front.* **2019**, *3*, 1510–1517.

(24) Wang, Y.; Tan, X.; Zhang, Y.-M.; Zhu, S.; Zhang, I.; Yu, B.; Wang, K.; Yang, B.; Li, M.; Zou, B.; et al. Dynamic Behavior of Molecular Switches in Crystal under Pressure and Its Reflection on Tactile Sensing. *J. Am. Chem. Soc.* **2015**, *137*, 931–939.

(25) Ma, Z.; Meng, X.; Ji, Y.; Li, A.; Qi, G.; Xu, W.; Zou, B.; Ma, Y.; Kuang, G.-C.; Jia, X. Pressure Induced the Largest Emission Wavelength Change in a Single Crystal. *Dyes Pigm.* **2019**, *162*, 136–144.

(26) Yue, M.; Wang, Y.; Wang, L.; Lin, X.; Li, K.; Zheng, H.; Yang, T. Pressure-induced Polymerization of Butyrdioic Acid and its Li⁺ Salt. *Chin. Chem. Lett.* **2018**, *29*, 328–330.

(27) Yang, X.; Wang, X.; Wang, Y.; Li, K.; Zheng, H. rom Molecules to Carbon Materials-High Pressure Induced Polymerization and Bonding Mechanisms of Unsaturated Compounds. *Crystals* **2019**, *9*, 490.

(28) Wang, X.; Li, K.; Zheng, H.; Zhang, P. Chemical Reactions of Molecules under High Pressure. *Chem. Bull.* **2019**, *82*, 387–398.

(29) Xu, J.; Semin, S.; Cremers, J.; Wang, L.; Savoini, M.; Fron, E.; Coutino, E.; Chervy, T.; Wang, C.; Li, Y.; et al. Controlling Microsized Polymorphic Architectures with Distinct Linear and Nonlinear Optical Properties. *Adv. Opt. Mater.* **2015**, *3*, 948–956.

(30) Xu, J.; Semin, S.; Niedzialek, D.; Kouwer, P. H. J.; Fron, E.; Coutino, E.; Savoini, M.; Li, Y.; Hofkens, J.; Uji-I, H.; et al. Self-Assembled Organic Microfibers for Nonlinear Optics. *Adv. Mater.* **2013**, *25*, 2084–2089.

(31) Duan, Y.; Ju, C.; Yang, G.; Fron, E.; Coutino-Gonzalez, E.; Semin, S.; Fan, C.; Balok, R. S.; Cremers, J.; Tinnemans, P.; et al. Aggregation Induced Enhancement of Linear and Nonlinear Optical Emission from a Hexaphenylene Derivative. *Adv. Funct. Mater.* **2016**, *26*, 8968–8977.

(32) Ju, C.; Li, X.; Yang, G.; Yuan, C.; Semin, S.; Feng, Y.; Rasing, T.; Xu, J. Polymorph Dependent Linear and Nonlinear Optical Properties of Naphthalenyl Functionalized Fluorenones. *Dyes Pigm.* **2019**, *166*, 272–282.

(33) Li, X.; Semin, S.; Estrada, L. A.; Yuan, C.; Duan, Y.; Cremers, J.; Tinnemans, P.; Kouwer, P.; Rowan, A. E.; Rasing, T.; et al. Strong Optical Nonlinearities of Self-assembled Polymorphic Microstructures of Phenylethynyl Functionalized Fluorenones. *Chin. Chem. Lett.* **2018**, *29*, 297–300.

(34) Yuan, M.-S.; Wang, D.-E.; Xue, P.; Wang, W.; Wang, J.-C.; Tu, Q.; Liu, Z.; Liu, Y.; Zhang, Y.; Wang, J. Fluorenone Organic Crystals: Two-Color Luminescence Switching and Reversible Phase Transformations between π - π Stacking-Directed Packing and Hydrogen Bond-Directed Packing. *Chem. Mater.* **2014**, *26*, 2467–2477.

(35) Mao, H. K.; Xu, J.; Bell, P. M. Calibration of the Ruby Pressure Gage to 800 kbar under Quasi-Hydrostatic Conditions. *J. Geophys. Res.* **1986**, *91*, 4673–4676.

(36) Prescher, C.; Prakapenka, V. B. DIOPTAS: a Program for Reduction of Two-Dimensional X-ray Diffraction Data and Data Exploration. *High Pressure Res.* **2015**, *35*, 223–230.

(37) Petricek, V.; Dusek, M.; Palatinus, L. Crystallographic Computing System JANA2006: General features. *Z. Kristallogr. - Cryst. Mater.* **2014**, *229*, 345–352.

(38) Frisch, M. J.; Trucks, G. W.; Schlegel, H. B.; Scuseria, G. E.; Robb, M. A.; Cheeseman, J. R.; Scalmani, G.; Barone, V.; Mennucci, B.; Petersson, G. A., et al. *Gaussian 09*, revision D.01; Gaussian, Inc.: Wallingford, CT, 2010.

(39) Lee, C.; Yang, W.; Parr, R. G. Development of the Colle-Salvetti Correlation-energy Formula into a Functional of the Electron Density. *Phys. Rev. B: Condens. Matter Mater. Phys.* **1988**, *37*, 785–789.

(40) Stephens, P. J.; Devlin, F. J.; Chabalowski, C. F.; Frisch, M. J. Ab Initio Calculation of Vibrational Absorption and Circular Dichroism Spectra Using Density Functional Force Fields. *J. Phys. Chem.* **1994**, *98*, 11623–11627.

(41) Gong, X.; Xiao, H.; van de Graaf, B. Ab Initio Studies on Four Alkyl Nitric Esters. *J. Mol. Struct.: THEOCHEM* **1997**, *393*, 207–212.

(42) Wang, J.; Gu, X.; Zhang, P.; Huang, X.; Zheng, X.; Chen, M.; Feng, H.; Kwok, R. T. K.; Lam, J. W. Y.; Tang, B. Z. Ionization and Anion- π^* Interaction: A New Strategy for Structural Design of Aggregation-Induced Emission Luminogens. *J. Am. Chem. Soc.* **2017**, *139*, 16974–16979.

(43) Bandyopadhyay, A.; Ghosh, D.; Pati, S. K. Shining Light on New-Generation Two-Dimensional Materials from a Computational Viewpoint. *J. Phys. Chem. Lett.* **2018**, *9*, 1605–1612.